J|A|C|S
ARTICLES
Published on Web 08/17/2002

In Situ Raman Spectroelectrochemistry of Electron Transfer between Glassy Carbon and a Chemisorbed Nitroazobenzene Monolayer

Takashi Itoh† and Richard L. McCreery*,‡

Contribution from the Department of Chemistry, The Ohio State University, 100 West 18th Avenue, Columbus, Ohio 43210, and Department of Applied Chemistry, Tohoku University, Japan

Received March 18, 2002

Abstract: In situ Raman spectroscopy was used to monitor 4-nitroazobenzene (NAB) in an electrochemical cell, both as a free molecule and as a chemisorbed monolayer on a glassy carbon (GC) electrode surface. Reduction of free NAB exhibited two well-defined voltammetric couples in acetonitrile, and the accompanying spectral changes supported a mechanism involving two successive 1-e^- transfers. Raman spectra of NAB chemisorbed to GC via diazonium ion reduction were obtained in acetonitrile with a high-sensitivity, line-focused CCD spectrometer. The chemisorbed NAB spectra were quite different from the free NAB spectra, and were sufficiently strong to monitor as a function of applied potential. In the potential range of +400 to −800 mV vs Ag/Ag^+, the intensity of the Raman bands associated with the phenyl−NO_2 moiety varied, implying an electronic interaction between the π system of the graphitic substrate and the chemisorbed NAB molecules. Negative of −800 mV, a 1-e^- voltammetric reduction peak was observed, which was reversible on the positive voltage scan. This peak was accompanied by significant spectral changes, particularly the loss of the N═N and NO_2 stretches. The spectra are consistent with formation of a quinoid structure containing a C═C double bond between the NAB and the graphitic surface. The electron transfer and spectral changes occurred over a wider potential range than expected for a conventional Nernstian equilibrium, but did not appear to be broadened by slow electron-transfer kinetics. The results imply a significant perturbation of electron transfer between the GC and the monolayer, caused by strong electronic coupling between the graphitic π system and the NAB orbitals. Rather than a discrete electron transfer to a free molecule, the electron transfer to chemisorbed NAB is more gradual, and is presumably driven by the electric field at the electrode/solution interface.

Introduction

The motivation for the spectroscopic examination of carbon electrode surfaces described herein is derived from three rather disparate fields. First, graphitic carbon is a widely used electrode material in batteries, fuel cells, electrosynthesis, and electroanalysis, and its electrochemical properties are determined in part by surface chemistry.[1−3] Second, a succession of technical advances in surface vibrational spectroscopy has enabled surface structure to be investigated with infrared and Raman spectroscopy, often directly in the electrolyte of interest.[4−9] Third, recent developments in molecular electronics have demonstrated the importance of electronic coupling between a conductor and a molecule or collection of molecules, to exploit molecules as components in electronic circuits.[10−14] For example, much of the behavior of a "molecular junction", consisting of a molecular monolayer positioned between two conductors,[15,16] is controlled by the nature of the molecule/conductor interface, which is in turn controlled by the electronic coupling between the orbitals in the molecule and the electronic states in the conductor.[17,18]

* Address correspondence to this author. E-mail: mccreery.2@osu.edu.
† Tohoku University.
‡ The Ohio State University.

(1) McCreery, R. L. Carbon Electrodes: Structural Effects on Electron Transfer Kinetics. In *Electroanalytical Chemistry*; Bard, A. J., Ed.; Dekker: New York, 1991; Vol. 17, p 221.
(2) Kinoshita, K. *Carbon, Electrochemical and Physicochemical Properties*; John Wiley and Sons: New York, 1988.
(3) McCreery, R. L.; Cline, K. K. *Carbon Electrodes*; Dekker: New York, 1996.
(4) Birke, R. L.; Lombardi, J. R. Surface-Enhanced Raman Scattering. In *Spectroelectrochemistry: Theory and Practice*; Gale, R. J., Ed.; Plenum Press: New York, 1988; p 263.
(5) McCreery, R. L. *Raman Spectroscopy for Chemical Analysis*; John Wiley: New York, 2000; Vol. 157.
(6) Kambhampati, P.; Child, C. M.; Foster, M. C.; Campion, A. *J. Chem. Phys.* **1998**, *108*, 5013.
(7) Kambhampati, P.; Campion, A. *Surf. Sci.* **1999**, *427−428*, 115.
(8) Freunsch, P.; Van Duyne, R. P.; Schneider, S. *Chem. Phys. Lett.* **1997**, *281*, 372.
(9) Van Duyne, R. P.; Haushalter, J. P. *J. Phys. Chem.* **1984**, *88*, 2446.
(10) Jortner, J.; Ratner, M. *Molecular Electronics*; Blackwell Science Ltd.: Cambridge, MA, 1997.
(11) Reed, M. A.; Tour, J. M. *Sci. Am.* **2000**, 86.
(12) Yaliraki, S. N.; Kemp, M.; Ratner, M. A. *J. Am. Chem. Soc.* **1999**, *121*, 3428.
(13) Mujica, V.; Roitberg, A. E.; Ratner, M. A. *J. Phys. Chem.* **2000**, *112*, 6834.
(14) Reed, M. A.; Chen, J.; Rawlett, A. M.; Price, D. W.; Tour, J. M. *Appl. Phys. Lett.* **2001**, *78*, 3735.
(15) Slowinski, K.; Majda, M. *J. Electroanal. Chem.* **2000**, *491*, 139.
(16) Holmlin, R. E.; Haag, R.; Chabinyc, M. L.; Ismagilov, R. F.; Cohen, A. E.; Terfort, A.; Rampi, M. A.; Whitesides, G. M. *J. Am. Chem. Soc.* **2001**, *123*, 5075.

10.1021/ja020398u CCC: $22.00

Optical spectroscopy has been used since the 1960s to probe electrochemical interfaces in situ, under the general designation of "spectroelectrochemistry". UV−vis, FTIR, and Raman spectroscopies provide information about molecular structure, which is difficult to obtain by electrochemical techniques alone. Of particular relevance is in situ Raman spectroscopy, which is especially informative about carbon electrode surfaces and provides insights into molecular structural changes associated with electrochemical charge transfer.[4,5,8,19,20] In situ Raman spectroscopy has been used for monitoring electrogenerated reactive intermediates, as well as adsorbates on metal and carbon surfaces. Since carbon electrodes do not support electromagnetic (EM) field enhancement, which is a large factor in surface-enhanced Raman spectroscopy, Raman spectroscopy of carbon surfaces depends on very sensitive spectrometers incorporating CCD detectors.[21−24] While Raman spectra of monolayers bonded to carbon surfaces have been obtained in air and vacuum without any known EM field enhancement, spectra of monolayers on carbon in an electrolyte solution have not been reported, to our knowledge.

Electronic coupling between adsorbates and electrode materials has been examined in several contexts, often in an electrolyte solution. A variety of spectroscopic investigations of the interactions of adsorbates with metal surfaces have been reported, based on infrared, Raman, UV−vis reflectance, and fluorescence spectroscopies as well as UHV surface science and electrochemical probes.[7,25−32] Electron transfer from a metal to a tethered redox center has been examined in many laboratories, often involving self-assembled monolayers on gold surfaces.[33−39] For aliphatic tethers, electronic coupling is weak, and tunneling through the aliphatic chain controls electron transfer. For conjugated tethers such as *p*-phenylenevinyl oligomers, tunneling is much faster, and the electron-transfer rate is weakly dependent on the oligomer length.[33] Carbon electrodes have been studied rarely in the context of electron transfer through surface monolayers, but unusually efficient tunneling was observed for conjugated monolayers on glassy carbon.[40] Charge transfer through monolayers in electrochemical cells is closely related to conductivity in molecular junctions, since both involve transport of electrons (or holes) across a monolayer bonded to a conductor. In both cases, the degree of electronic coupling is a critical parameter for determining the rate of electron transfer.

In addition to our ongoing interest in carbon electrochemistry and modified carbon electrodes, we recently reported a carbon-based molecular junction which exhibited "conductance switching".[41,42] Application of a negative bias to the carbon substrate caused a 47 Å thick layer of covalently bonded nitroazobenzene to switch into a high-conductance state, and the conductance change could be reversed with a positive bias. Previous ex situ Raman investigations of 4-nitroazobenzene (NAB)-modified glassy carbon (GC) implied strong electronic coupling between the NAB and carbon, with a major increase in the Raman cross section occurring upon NAB chemisorption.[22,43] Since the NAB layer is sandwiched between two opaque contacts (mercury and graphitic carbon) in the molecular junction, it was not possible to probe structural changes associated with conductance switching. In a broader context, the mechanism of conductance switching in metal/monolayer/metal junctions studied with STM and *i*/*V* curves is uncertain and somewhat controversial.[14,44−48]

In the current investigation we use in situ Raman spectroelectrochemistry to investigate NAB chemisorbed on GC in an electrochemical cell. Application of a potential permitted generation of a high electric field across the monolayer, and structural changes in the NAB were deduced from the in situ Raman spectrum. To our knowledge, the in situ Raman spectra are the first reported for monolayers on carbon without the benefit of EM field enhancement. Raman spectra from the NAB-modified GC surface during application of negative potentials are compared to spectra obtained from solution-phase NAB during electrochemical reduction. The results reveal unusual interactions between the NAB and the graphitic π system, which may be unique to aromatic monolayers covalently bonded to and conjugated with graphitic electronic conductors.

Experimental Section

Raman spectra were recorded with a custom line-focused f/2 Raman spectrometer (Chromex) and back-thinned CCD (Andor) described elsewhere.[21] The 514.5 nm laser was incident at 45° to the electrode surface, and scattered light was collected normal to the surface. The focal line had dimensions of approximately 50 μm × 5 mm at the electrode. The electrode was positioned parallel to a sapphire window,

(17) Hong, S.; Reifenberger, R.; Tian, W.; Datta, S.; Henderson, J.; Kubiak, C. P. *Superlattices Microstruct.* **2000**, *28*, 289.
(18) Tian, W.; Datta, S.; Hong, S.; Reifenberger, R.; Henderson, J. I.; Kubiak, C. P. *J. Chem. Phys.* **1998**, *109*, 2874.
(19) Van Duyne, R. P.; Hulteen, J. C.; Treichel, D. A. *J. Chem. Phys.* **1993**, *99*, 2101.
(20) Yang, W.-h.; Hulteen, J. C.; Schatz, G. C.; Van Duyne, R. P. *J. Chem. Phys.* **1996**, *104*, 4313.
(21) Ramsey, J. D.; Ranganathan, S.; Zhao, J.; McCreery, R. L. *Appl. Spectrosc.* **2001**, *55*, 767.
(22) Liu, Y.-C.; McCreery, R. L. *Anal. Chem.* **1997**, *69*, 2091.
(23) Zhao, J.; McCreery, R. L. *Langmuir* **1995**, *11*, 4036.
(24) Liu, Y.-C.; McCreery, R. L. *J. Am. Chem. Soc.* **1995**, *117*, 11254.
(25) Lecomte, S.; Matejka, P.; Baron, M. H. *Langmuir* **1998**, *14*, 4373.
(26) Liu, Y.-C. *Langmuir* **2002**, *18*, 174.
(27) Weaver, M. J.; Wasileski, S. A. *Langmuir* **2001**, *17*, 3039.
(28) Wasileski, S. A.; Koper, T. M.; Weaver, M. J. *J. Am. Chem. Soc.* **2002**, *124*, 2796.
(29) Henglein, F.; Kolb, D. M.; Stolberg, L.; Lipkowski, J. *Surf. Sci.* **1993**, *291*, 325.
(30) Franke, C.; Piazza, G.; Kolb, D. M. *Electrochim. Acta* **1989**, *34*, 67.
(31) Plieth, W. J.; Schmidt, P.; Keller, P. *Electrochim. Acta* **1986**, *31*, 1001.
(32) Pope, J. M.; Buttry, D. A. *J. Electroanal. Chem.* **2001**, *498*, 75.
(33) Sikes, H. D.; Smalley, J. F.; Dudek, S. P.; Cook, A. R.; Newton, M. D.; Chidsey, C. E. D.; Feldberg, S. W. *Science (Washington, D.C.)* **2001**, *291*, 1519.
(34) Barrelet, C. J.; Robinson, D. B.; Cheng, J.; Hunt, T. P.; Quate, C. F.; Chidsey, C. E. D. *Langmuir* **2001**, *17*, 3460.
(35) Sachs, S. B.; Dudek, S. P.; Hsung, R. P.; Sita, L. R.; Smalley, J. F.; Newton, M. D.; Feldberg, S. W.; Chidsey, C. E. D. *J. Am. Chem. Soc.* **1997**, *119*, 10563.
(36) Finklea, H. O. Electrochemistry of Organized Monolayers of Thiols and Related Molecules on Electrodes. In *Electroanalytical Chemistry*; Bard, A. J., Ed.; Dekker: New York, 1996; Vol. 19, p 109.
(37) Creager, S.; Yu, C. J.; Bamdad, C.; O'Connor, S.; MacLean, T.; Lam, E.; Chong, Y.; Olsen, G. T.; Luo, J.; Gozin, M.; Kayyem, J. F. *J. Am. Chem. Soc.* **1999**, *121*, 1059.
(38) Sumner, J. J.; Weber, K. S.; Hockett, L. A.; Creager, S. E. *J. Phys. Chem.* **2000**, *104*, 7449.
(39) Alleman, K. S.; Weber, K.; Creager, S. *J. Phys. Chem.* **1996**, *100*, 17050.
(40) Yang, H.-H.; McCreery, R. L. *Anal. Chem.* **1999**, *71*, 4081.
(41) Ranganathan, S.; Steidel, I.; Anariba, F.; McCreery, R. L. *Nano Lett.* **2001**, *1*, 491.
(42) Solak, A. O.; Ranganathan, S.; T., I.; McCreery, R. L. *Electrochem. Solid State Lett.* **2002**, *5*, E43.
(43) Kuo, T.-C. Raman Spectroscopy and Electrochemistry of Modified Carbon Surfaces. Ph.D. Thesis, The Ohio State University, Columbus, OH, 1999.
(44) Donhauser, Z. J.; Mantooth, B. A.; Kelly, K. F.; Bumm, L. A.; Monnell, J. D.; Stapleton, J. J.; Price, D. W.; Rawlett, A. M.; Allara, D. L.; Tour, J. M.; Weiss, P. S. *Science (Washington, D.C.)* **2001**, *292*, 2303.
(45) Cygan, M. T.; Dunbar, T. D.; Arnold, J. J.; Bumm, L. A.; Shedlock, N. F.; Burgin, T. P.; Jones, L.; Allara, D. L.; Tour, J. M.; Weiss, P. S. *J. Am. Chem. Soc.* **1998**, *120*, 2721.
(46) Zhou, C.; Deshpande, M. R.; Reed, M. A.; Jones, L.; Tour, J. M. *Appl. Phys. Lett.* **1997**, *71*, 661.
(47) Bredas, J. L.; Beljonne, D.; Cornil, J.; Calbert, J. P.; Shuai, Z.; Silbey, R. *Synth. Met.* **2002**, *125*, 107.
(48) Karzazi, Y.; Cornil, J.; Bredas, J. L. *J. Am. Chem. Soc.* **2001**, *123*, 10076.

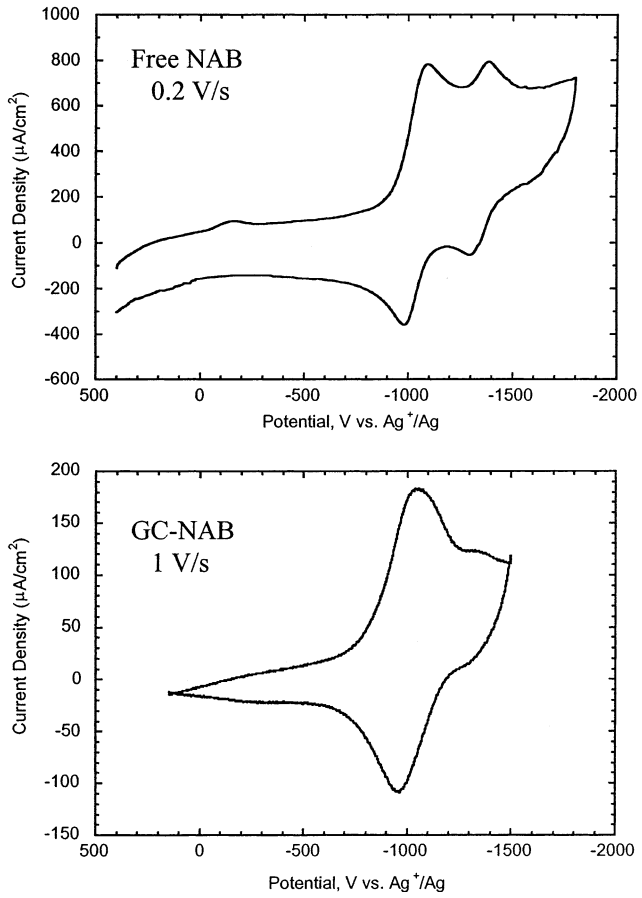

Figure 1. Top: Voltammetry of 1 mM NAB dissolved in 1 M $TBABF_4$ in acetonitrile at a 0.07 cm^2 GC electrode. Scan rate: 0.2 V/s. Bottom: Voltammetry of an NAB monolayer on GC, in 1 M $TBABF_4$ in acetonitrile, 1 V/s. A background scan using an unmodified GC electrode was subtracted before plotting.

with an approximately 1 mm thickness of solution between the window and electrode surface. The electrode potential was controlled with a conventional three-electrode potentiostat [Bioanalytical Systems (PWR-3 or 100S)] using a Pt wire auxiliary electrode and a Ag/Ag^+ (0.01 M) reference electrode.

A $6 \times 4 \times 1.5$ mm^3 working electrode was made from a GC plate (Tokai, GC-20), with an effective area in contact with the electrolyte of 24 mm^2. The GC was polished on a polishing cloth using an alumina slurry with successive 1.0, 0.3, and 0.05 μm particle sizes and then cleaned ultrasonically in "NANOpure" 18 MΩ water (Barnstead). This GC was mounted on a Pyrex electrode holder by silicone resin to avoid epoxy contamination. 4-Nitroazobenzene was chemisorbed to the GC surface by electrochemical reduction of 1.0 mM 4-nitro 4′-diazonium azobenzene tetrafluoroborate in acetonitrile containing 1.0 M tetrabutylammonium tetrafluoroborate ($TBABF_4$) as described previously.[49] The high $TBABF_4$ concentration reduced ohmic potential errors in the thin-layer spectroelectrochemical cell. To avoid multilayer formation, the derivatization scan consisted of one cycle from +400 to −800 mV vs Ag/Ag^+ at 200 mV/s. Modified electrodes were sonicated in acetonitrile for 5 min before the spectroelectrochemical experiments.

Solutions were thoroughly degassed before the electrochemical experiments, and the spectroelectrochemical cell was blanketed with dry N_2 continuously. Residual O_2 interfered with the voltammetry, and also appeared to react with electrogenerated products, so care was taken to minimize oxygen contamination. During examination of the NAB-modified GC (referred to as "GC−NAB") the electrolyte was 1.0 M

(49) DuVall, S.; McCreery, R. L. *J. Am. Chem. Soc.* **2000**, *122*, 6759.

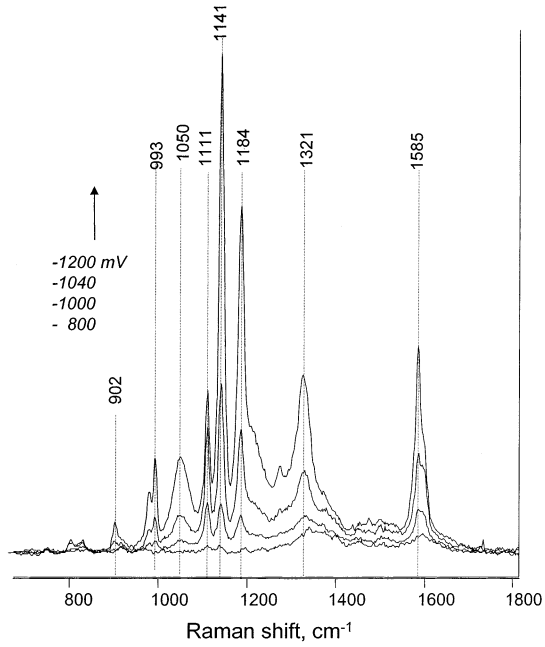

Figure 2. Raman spectra of 1 mM free NAB in 1 M $TBABF_4$/acetonitrile during application of fixed potentials at a GC electrode. The spectrum acquired at +400 mV showed only acetonitrile and GC bands, and was subtracted from each spectrum shown. The four spectra (from bottom to top) were acquired with 8.2 mW of 514.5 nm laser power and 100 s of CCD integration time and at potentials of −800, −1000, −1040, and −1200 mV.

$TBABF_4$ in acetonitrile. Initial experiments were conducted with 1 mM NAB ("free NAB") in acetonitrile containing 1 M $TBABF_4$, and an unmodified GC electrode. Voltammetry was conducted with a commercial GC 20 electrode having a 0.07 cm^2 area.

Gaussian 98 using density functional theory with a 6-31 G basis set [B3LYP/6-31G(d)] was used to predict vibrational frequencies and bond lengths. For all frequencies cited below, the Gaussian frequency was multiplied by a scaling factor of 0.9613.

Results

The voltammetry and spectroelectrochemistry of free NAB in acetonitrile were examined first, to compare to those of chemisorbed NAB. The voltammogram in Figure 1 shows two quasireversible waves, centered at −1036 mV ($\Delta E_p = 102$ mV) and −1341 mV ($\Delta E_p = 88$ mV). Raman spectra were obtained under potential control from a thin layer of NAB solution adjacent to a GC electrode. An initial check on the stability of the reduction products was made by obtaining a succession of spectra at a fixed potential, with each spectrum requiring 100 s and spaced at intervals of 30 s. For potentials of −1000 and −1400 mV vs Ag/Ag^+, a sequence of 50 spectra showed no trend in Raman intensity with time, only random variation of approximately ±10%. This observation indicates that both of the reduction products implied by Figure 1 are stable with time and laser exposure, for at least 1 h.

The progression of the in situ Raman spectrum of NAB with a negative potential sequence is shown in Figure 2. The reduction product is resonance enhanced, and has a much stronger spectrum than the initial NAB solution. The spectra in Figure 2 are differences between the spectra obtained at the indicated potentials and the spectrum at +400 mV. This subtraction removes the acetonitrile bands and any contributions from the window and GC. Spectra of NAB were obtained

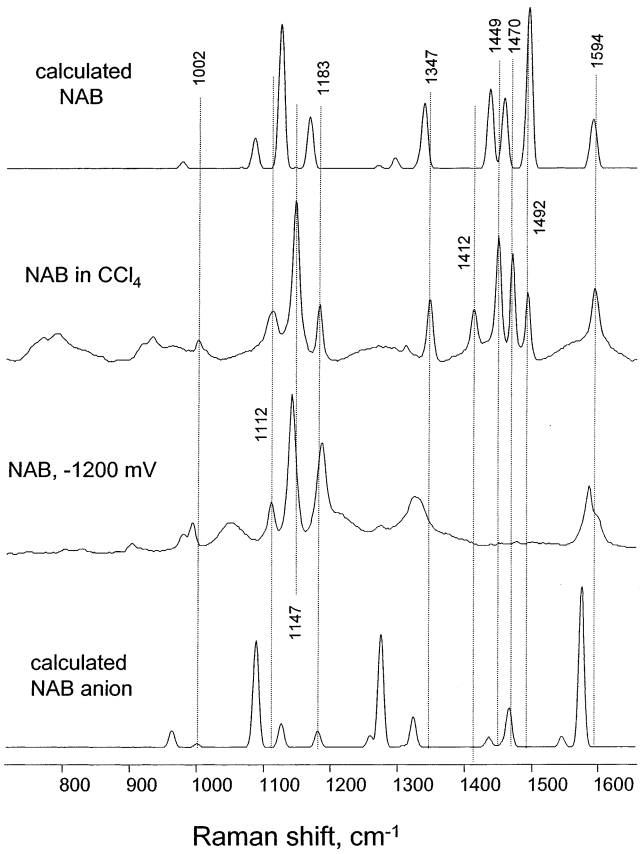

Figure 3. Calculated spectra for NAB and NAB anion compared to that for free NAB in CCl_4 and the −1200 mV spectrum from Figure 2. Calculated spectra arbitrarily assumed a 10 cm^{-1} line width. Vertical lines and frequencies are those observed for NAB in solution.

Table 1. Peak Frequencies and Assignments for NAB in Solution

calcd[a] for free NAB	free NAB in CCl_4	NAB anion in CH_3CN, 1200 mV	calcd for NAB anion[a]	assignment[b]
1007	1002	993	1001	ring B deformation
1085	1112	1111	1107	phenyl−NO_2 stretch (43)
1125	1147	1141	1126	phenyl−NN stretch (44)
1172	1183	1184	1181	CH bend (47)[c]
1339	1347	1321	1324	NO_2 stretch (53)
1394	1412			N═N + ring A (54)
1454	1449		1444[d]	N═N stretch (56)
1472	1470		1456[d]	phenyl−NN stretch + ring deformation (57)
1494	1492			N═N stretch (58)
1594	1594	1585	1584	CC stretch, ring A (62)

[a] Gaussian 98, B3LYP/6-31G(d), scaling factor of 0.9613. [b] The mode number for NAB is in parentheses; "ring A" refers to the phenyl ring with NO_2, and "ring B" refers to the phenyl ring opposite the NO_2 group. [c] Includes the N−N stretch in the anion. [d] Nearest calculated band.

separately at higher concentration in both CCl_4 and acetonitrile. The spectra were very similar except for solvent bands, and the CCl_4 spectrum is shown in Figure 3, along with the in situ spectrum at −1200 mV. Peak frequencies and assignments for NAB and NAB anion are listed in Table 1. Also shown in Figure 3 are calculated spectra for both NAB and its anion radical. The complete loss of N═N vibrations (1400−1500 cm^{-1}) upon reduction and the major change in the NO_2 stretch (1347 cm^{-1}) indicate significant structural differences between NAB and its first reduction product.

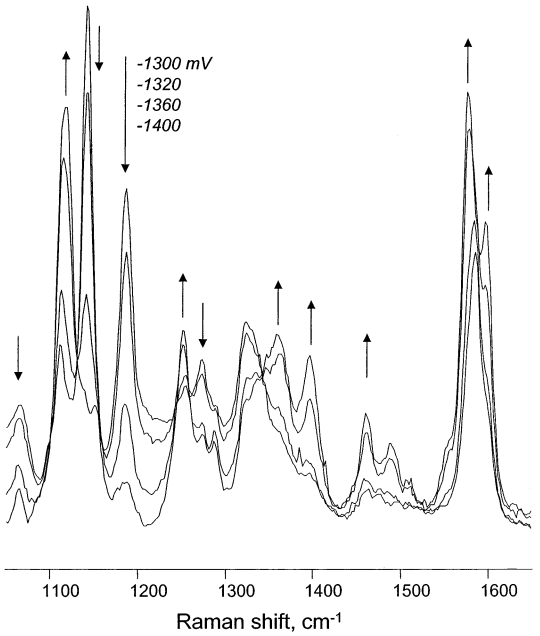

Figure 4. In situ spectra of free NAB similar to those of Figure 2, but for more negative potentials. Arrows indicate the direction of the intensity changes as the applied potential is stepped in the sequence −1300, −1320, −1380, and −1400 mV. Other conditions are the same as those in Figure 2.

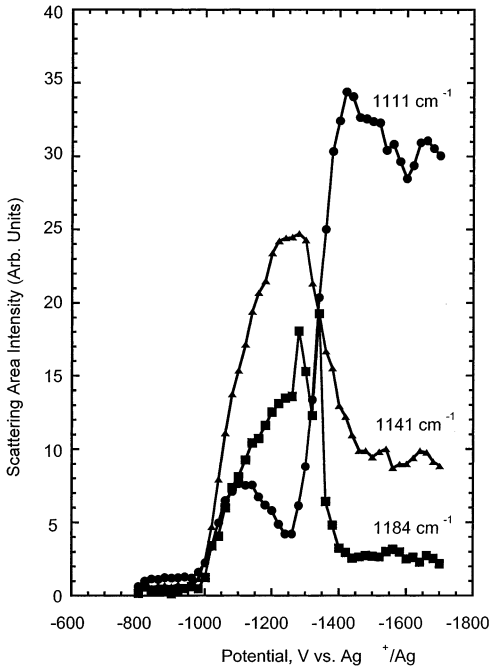

Figure 5. Intensities of the 1118, 1140, and 1184 cm^{-1} bands from Figures 2 and 4, relative to a +400 mV baseline, and as a function of applied potential.

The sequence of in situ spectra was continued to potentials negative of −1200 mV as shown in Figure 4. When the potential proceeds negative of the first voltammetric peak, the 1141 and 1184 cm^{-1} intensities decrease, that of 1111 cm^{-1} increases, and new bands appear at 1395, 1459, and 1489 cm^{-1}. The intensities of the 1118, 1141, and 1184 cm^{-1} bands were analyzed in detail by deconvolution, to provide band areas and band centers as functions of potential. Figure 5 shows a plot of band intensity vs potential for in situ spectra obtained with free NAB. In addition to the starting NAB, which does not contribute

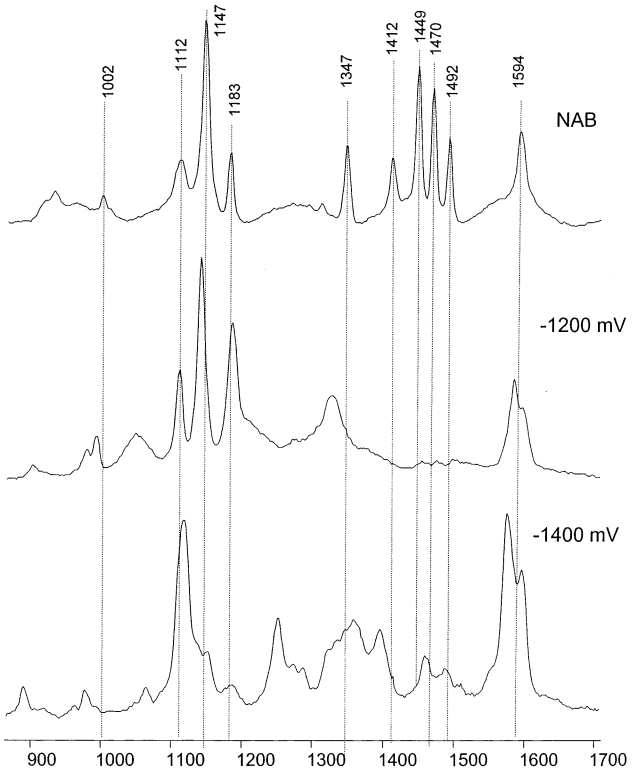

Figure 6. Comparison of the free NAB spectrum in CCl_4 with in situ spectra in acetonitrile at −1140 and −1400 mV. Other conditions are the same as in Figure 2.

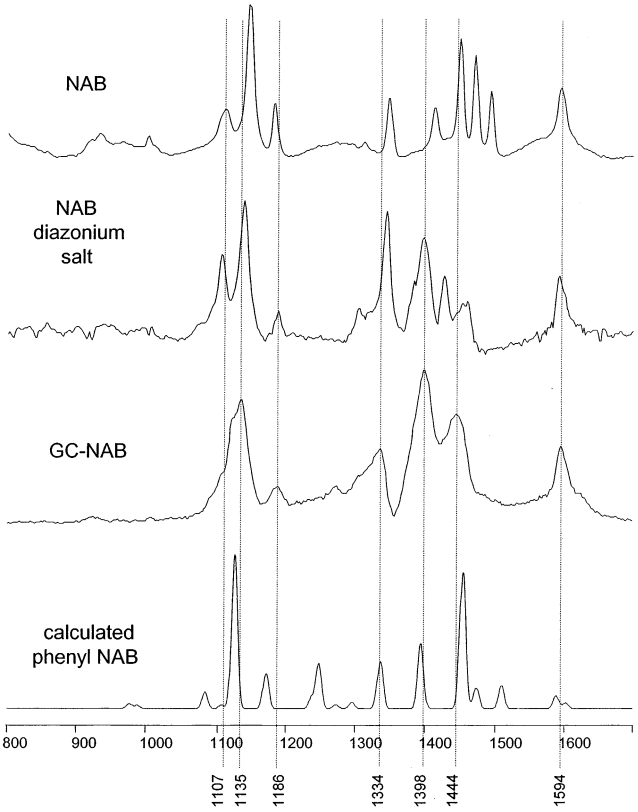

Figure 7. Raman spectra of NAB in CCl_4, NAB 4′-diazonium salt dissolved in acetonitrile, and NAB-modified GC observed in air and the calculated spectrum for 4′-phenyl-NAB. Vertical lines and labels refer to the chemisorbed NAB spectrum. A GC background was subtracted from the GC−NAB spectrum before plotting.

due to its much weaker scattering, there are two observable reduction products. The spectra at −1200 and −1400 mV represent the Raman scattering from primarily the first product (with a strong 1184 cm^{-1} band) and the second (with a strong 1118 cm^{-1} band), respectively. These spectra are compared to that of NAB in Figure 6.

Inspection of the in situ spectra reveals that the 1184 cm^{-1} peak is solely associated with the first reduction product, while the 1118 cm^{-1} band is predominantly due to the second product. Assuming that the maximum intensity of the 1184 cm^{-1} band represents the case where all NAB is in the form of the first reduction product, the oxidation/reduction (ox/red) ratio may be determined as a function of potential, as $(I_{1141}{}^{max} - I_{1141})/I_{1141}$. A plot of E vs log(ox/red) for the 1141 cm^{-1} band has a slope of 85 mV with an intercept of −1076 mV. A similar plot for the 1111 cm^{-1} had a slope of 60 mV and intercept of −1321 mV, while the plot for 1184 cm^{-1} had a slope of 95 and intercept of −1073 mV. These results are consistent with two 1-e^- transfers with $E^{\circ\prime}$ values of −1.075 and −1.321 V vs Ag/Ag^+.

The spectrum of NAB chemisorbed to GC via reduction of the corresponding diazonium ion has been reported previously,[22] but was investigated here in more detail. Figure 7 shows spectra of NAB, its diazonium salt, NAB chemisorbed to GC, and a calculated spectrum for a model structure, 4′-phenyl-NAB. The 2307 cm^{-1} band of the N_2^+ group in the NAB diazonium ion is not on scale in Figure 7, but we verified that it vanished completely when the diazonium ion was reduced to N_2 and chemisorbed NAB. The voltammogram of the NAB−GC surface after rinsing and placing NAB−GC in blank electrolyte is shown in the lower trace of Figure 1. The initial reduction occurs at approximately the same potential as that of NAB, but appears to be one drawn out peak rather than two discrete peaks. The secondary redox couple apparent at about −1.2 V is much smaller than the main couple, and may be due to residual dissolved oxygen. The small current for the chemisorbed NAB monolayer above the background makes quantitative analysis difficult, but the approximate area under the reduction peak above the background corresponds to $(4.3 \pm 1.3) \times 10^{-5}$ C/cm^2 for the reduction and $(4.3 \pm 1.1) \times 10^{-5}$ C/cm^2 for the oxidation, for scan rates between 0.1 and 1.0 V/s. The coverage of NAB on glassy carbon has been reported to be in the range of 1.4×10^{-10} mol/cm^2 up to the 10×10^{-10} mol/cm^2 predicted for a close-packed monolayer,[24] while nitrophenyl monolayers prepared similarly have a coverage of 4.3×10^{-10} mol/cm^2. A subsequent XPS study narrowed this range to $(3.4-6.7) \times 10^{-10}$ mol/cm^2.[43] Although the uncertainty in coverage prevents a precise determination of the number of electrons transferred per chemisorbed NAB molecule, the range of $(3.4-6.7) \times 10^{-10}$ mol/cm^2 corresponds to a range of 0.67−1.3 e^- per chemisorbed NAB. Within the range of 0.1−1.0 V/s, the peak current for GC−NAB was linear with scan rate, and ΔE_p increased only slightly, from 113 to 130 mV.

The effects of applied potential on the in situ Raman spectra of chemisorbed NAB are shown in Figure 8. Although NAB features are apparent above the scattering from GC and acetonitrile, the raw spectra are difficult to analyze with these interferences present. The Raman difference spectrum calculated from the raw spectra at +400 and −1000 mV shown in Figure 8 demonstrates removal of solvent and GC bands, and highlights spectral changes with potential. A detailed sequence of difference spectra is shown in Figures 9 and 10, using the +400 mV

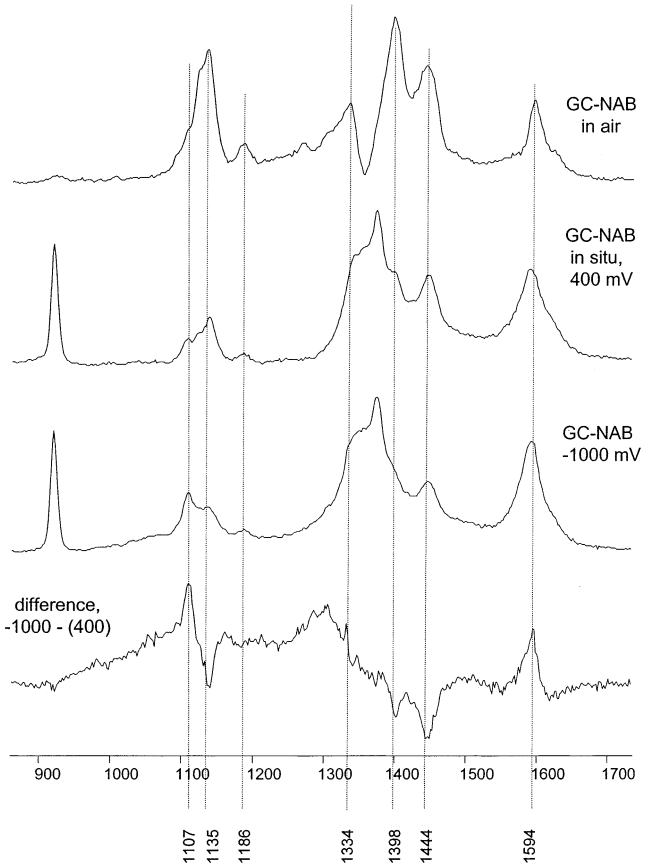

Figure 8. In situ Raman spectra of GC−NAB at +400 and −1000 mV, compared to that of GC−NAB in air. The bottom spectrum is the difference between the second and third spectra, showing only spectral changes caused by a potential step from +400 to −1000 mV. The saser power was 8.2 mW. The CCD integration time was 100 s.

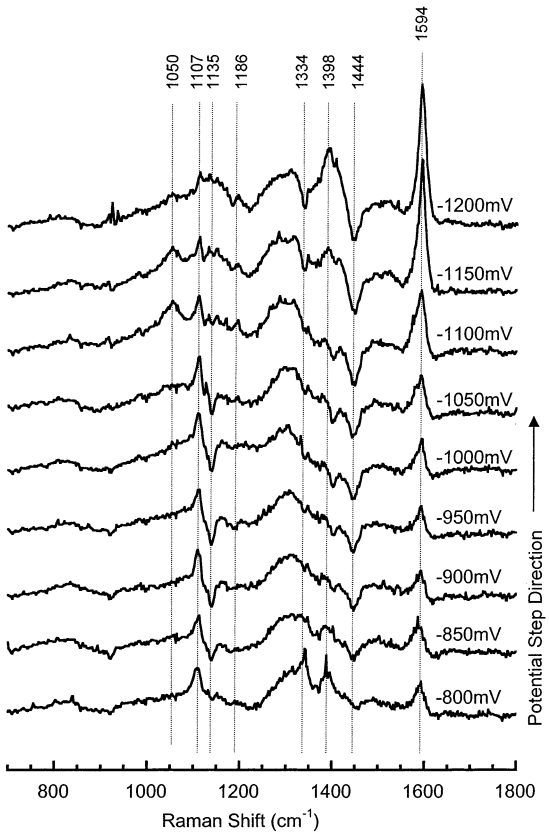

Figure 9. Difference spectra determined as shown in Figure 8, with the +400 mV spectrum as a reference. The spectra were obtained in the order shown, with 100 s for each CCD integration. Vertical lines and labels are positioned at frequencies observed for GC−NAB in air.

spectrum as the reference. The difference spectra reveal increases in peak intensity when the potential is stepped from +400 to −800 mV vs Ag/Ag^+ and then larger changes at more negative potential. Between +400 and −800 mV, there are gains in the 1594, 1398, 1334, and 1107 cm^{-1} intensities, while the remaining band intensities are nearly constant, and these changes occur gradually until the potential reaches −800 mV. As the potential becomes negative of −800 mV, the 1108, 1134, 1334, and 1444 cm^{-1} bands show both gains and losses of intensity, while the 1594 cm^{-1} band gains intensity. Negative of −1050 mV, a new band appears at 1050 cm^{-1}, and the 1398 cm^{-1} band regains its lost intensity.

The spectral changes upon a potential excursion to −1200 mV are partly but not completely reversible, as shown by the difference spectra in Figure 10. The negative peak at 1340 cm^{-1} in the final spectrum at −800 mV indicates significant loss of peak intensity compared to the initial spectrum at −800 mV, and the 1398 cm^{-1} band appeared to gain intensity. Although these intensity changes were apparently permanent, they were not observed for other bands, implying that they did not result from a general loss of chemisorbed NAB. Furthermore, the fact that the reduction charge approximately equals the oxidation charge in Figure 1b argues against gross desorption or other irreversible reactions. For several other bands observed at −1200 mV, such as 1594, 1050, and 1142 cm^{-1}, the intensity returned to nearly its original value at −800 mV after the negative potential excursion.

Discussion

The voltammetry of free NAB in solution (Figure 1) implies two successive 1-e^- reductions to produce the NAB anion and NAB dianion. The peak potentials depend weakly on the scan rate, indicating reasonably fast electron-transfer kinetics and $E_{1/2}$ values of −1.07 and −1.33 V vs Ag^+/Ag for the first and second reductions, respectively. In situ Raman spectroscopy supports the conclusion that two reduction products are formed successively, both of which are much stronger Raman scatterers than the parent NAB. Figure 5 shows the potential dependence of three Raman bands from Figures 2 and 4. The 1141 and 1184 cm^{-1} bands are due primarily to NAB anion, while the 1111 cm^{-1} band is due mainly to NAB^{2-}. The apparent maximum in the 1111 cm^{-1} band at −1150 mV is due to overlapping of the 1111 cm^{-1} band of NAB^- and the 1117 cm^{-1} band of NAB^{2-}. A shift in the peak frequency of this band occurs with potential, from 1111 cm^{-1} for $E > -1240$ mV to 1117 cm^{-1} for $E < -1260$ mV. The E vs log(ox/red) plots determined from the Raman intensities at 1111, 1141, and 1184 cm^{-1} had slopes of 85, 60, and 95 mV, further supporting a sequence of two 1-e^- reductions. The $E^{\circ\prime}$ values from the plots, which represent equilibrium rather than voltammetric values, are in reasonable agreement with the $E_{1/2}$ values apparent in Figure 1.

The Raman spectral changes shown in Figure 2 accompanying reduction of NAB to its anion are dramatic, with complete loss of the N═N stretches (1400−1500 cm^{-1}) and downshifts of the NO_2 (1347 cm^{-1}) and phenyl C═C stretches (1598 cm^{-1}). Gaussian 98 was used to predict molecular geometries and vibrational frequencies, with the results tabulated in Table 3

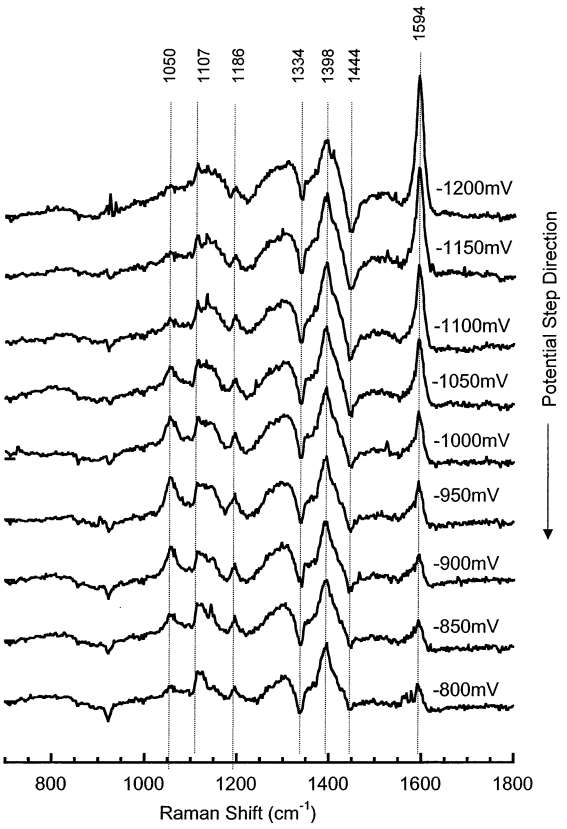

Figure 10. Same as Figure 9, but for increasing potential.

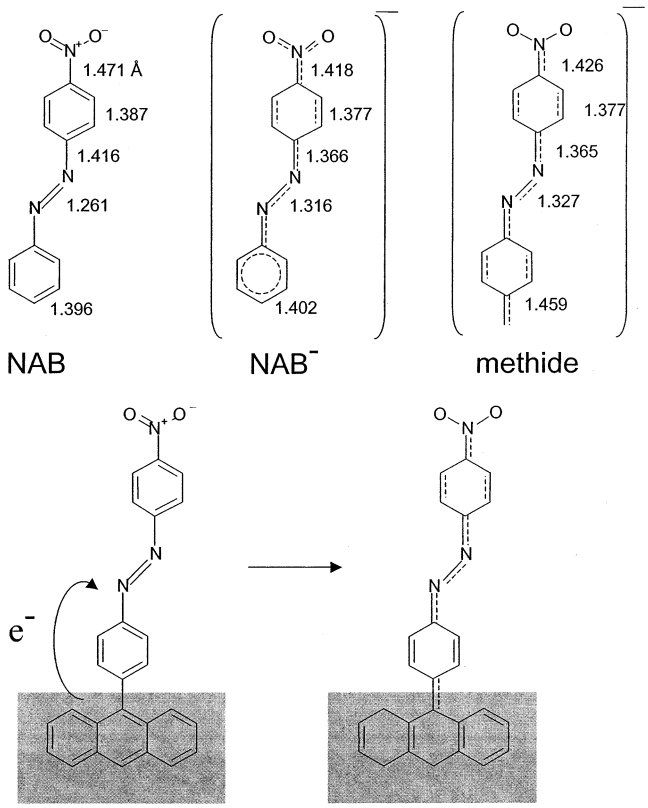

Figure 11. Structures of NAB, NAB radical anion, and NAB 4′-methide (top). Selected bond lengths from Gaussian 98 are shown for comparison. The reaction at the bottom is proposed to accompany electron transfer from GC to NAB.

Table 2. Peak Frequencies and Assignments for NAB Chemisorbed to Glassy Carbon

calcd[a] for 4′-phenyl-NAB	free NAB	NAB-N_2^+	NAB–GC	assignment[b]
1086	1112	1108	1107	phenyl−NO_2 stretch (59)
1127	1146	1139	1135	phenyl−NN stretch (62)
1172	1183	1189	1186	CH bend (65)
1247				CC bridging stretch (68)
1337	1346	1344	1334	NO_2 stretch (74)
1394	1411	1397	1398	N═N + ring A (76)
	1428[c]			
1454	1448	1454	1444	N═N stretch (79)
1510	1491			CC stretch, ring B (82)
1589	1594	1592	1594	CC stretch, ring A (86)

[a] Gaussian 98, B3LYP/6-31G(d), scaling factor of 0.9613. [b] The mode number for 4′-phenyl-NAB is in parentheses; "ring A" refers to the phenyl ring with NO_2, and "ring B" refers to the phenyl ring opposite the NO_2 group. [c] Observed for 4-substituted NAB derivatives, such as 4-nitro-4′-aminoazobenzene.

for bond lengths and frequencies of selected modes and molecules. Figure 3 shows Raman spectra of NAB and NAB^- determined from Gaussian 98 peak positions and intensities, after arbitrarily assuming bandwidths of 10 cm^{-1}. The calculated NAB features are in good agreement with those observed in CCl_4, and these spectra have been analyzed thoroughly by Biswas and Umapathy.[50] The short N−N bond length in NAB (1.261 Å) is consistent with its double bond character, and results in relatively high N−N stretching frequencies. Reduction to NAB^- causes major changes in bond lengths, with the C−NO_2 and C−NN bonds shortening and the N−N bond lengthening by about 0.05 Å. In addition, the C−NN stretching frequency increases, the NO_2 frequency decreases, and the N═N stretch decreases significantly. All of these bond length and frequency changes indicate the NAB takes on "quinoid" character when reduced, as shown in Figure 11. The electron is delocalized over most of the anion, and many of the bonds in the planar ring system have a bond order close to 1.5. Reduction of NAB^- to NAB^{2-} further emphasizes the quinoid structure, with a longer N−N bond and shorter C−NN and C−NO_2 bonds. Taking the electrochemical, spectroscopic, and theoretical results together, we conclude that NAB reduction in acetonitrile proceeds by two 1-e^- steps, with significant rearrangement of bonding and electron distribution.

Most of the substantial spectral changes accompanying chemisorption of NAB to GC are related to substitution at the 4′ position, para to the azo group. The spectrum of chemisorbed NAB matches most of the features in the 4′-diazonium salt of NAB, as shown in Figure 7 and listed in Table 2. The bands observed for GC−NAB correspond to those predicted theoretically for phenyl-NAB for the strongest features, with the exception of the bridging C−C band predicted at 1247 cm^{-1}. A bridging C−C mode was observed previously for phenyl rings chemisorbed to GC, but was quite weak.[22,24,43] On the basis of the vibrational modes calculated for phenyl-NAB, assignments were made to the strongest bands for GC−NAB, and are listed in Table 2.

The in situ spectroelectrochemical Raman spectra in Figures 8−10 differ from those obtained in air due to the presence of an applied potential. Not only might a potential cause redox reactions in the NAB monolayer but it also generates an electric field at the GC−solution interface. For chemisorbed molecules on metals studied by both IR and Raman spectroscopies, electric

(50) Biswas, N.; Umapathy, S. *J. Phys. Chem.* **2000**, *104*, 2734.

Table 3. Calculated[a] Bond Lengths and Vibrational Frequencies for Nitroazobenzene and Related Compounds

	NAB	NAB anion	NAB dianion	NAB methide	phenyl-NAB	phenyl-NAB anion
Bond Lengths (Å)						
N−O	1.231	1.255	1.281	1.249	1.231	1.252
C−NO_2	1.471	1.418	1.379	1.426	1.470	1.423
C−NN	1.416	1.366	1.329	1.365	1.417	1.367
N−N	1.261	1.316	1.368	1.327	1.264	1.318
C−C (bridging)				1.365	1.490	1.480
Predicted Vibrations[b] (cm^{-1})						
NO_2 stretch	1340	1324	1386	1313	1336	1311
N═N	1458	1181	1079	1262	1453	1259
phenyl−NN stretch	1124	1295	1385	1377	1127	1302
C═C stretch, ring A	1603	1584	1589	1587	1602	1583

[a] Gaussian 98, B3LYP/6-31G(d). [b] Scaling factor 0.9613.

fields can cause changes in frequency and intensity. In addition, electric fields at solid electrode surfaces in solution have been shown to affect UV−vis reflectance and fluorescence spectra.[45−48] For IR, such shifts have been interpreted as a vibrational Stark effect associated with the double-layer field,[27,51] while Raman intensity changes with potential have been associated with the chemical enhancement mechanism of surface-enhanced Raman scattering.[4,6,7,25,26,52] The intensity changes observed between +400 and −800 mV occur gradually over approximately 1 V of potential, and in the absence of a redox process observable by voltammetry. However, there is strong electronic coupling between the graphite and the monolayer through the conjugated C−C bond. Typical double-layer fields are in the region of 1 MV/cm, so some changes in electron distribution between the GC and the monolayer are likely when a potential is applied. It is interesting to note that only certain bands of the GC−NAB spectrum are enhanced as the potential becomes more negative. In particular, modes involving the NO_2 group (1107−1340 cm^{-1}) and the phenyl ring bonded to the NO_2 group (1398 and 1594 cm^{-1}) show a potential-induced enhancement. It is quite possible that a negative GC surface is driving electron density onto the phenyl−NO_2 moiety, and possibly shifting the molecular absorption band closer to the laser frequency by modifying the electrode to NAB charge-transfer absorption band.

As the potential approaches −1000 mV, electrons are transferred into the NAB layer to produce the reduction peak apparent in Figure 1. Accompanying reduction are loss of the N═N and NO_2 stretches, plus changes in the C−H band at 1140 cm^{-1}. Given the likelihood of resonance effects and the contribution of several bonds in the NAB to each mode, it is not yet possible to reliably associate potential-dependent intensity changes with particular changes in molecular structure. However, two conclusions are clear from the comparison of the NAB−GC spectra (Figures 9 and 10) to the free NAB spectra (Figures 2−6). First, modes in GC−NAB associated with N═N and NO_2 groups are significantly perturbed by reduction. Second, the intensity changes in GC−NAB, which occur negative of −800 mV, are quite different from those accompanying generation of NAB^- or NAB^{2-} from free NAB in solution. Free NAB exhibited loss of the azo modes, a downshift of the 1594 cm^{-1} and NO_2 bands, and significant resonance enhancement of all bands upon reduction to the anion. NAB−GC also exhibits loss of the N═N mode upon reduction, but no downshift of the 1594 cm^{-1} band and weak enhancement of only the 1594 cm^{-1} mode. A structure which is likely to be involved during NAB−GC reduction is NAB 4′-methide, shown in Figure 11. This structure is a model for NAB bonded to a graphitic sheet, in which the bonding to the NAB has been modified to the quinoid form. The methide structure forces the N−N bond to take on single bond character, and the phenyl−NN and phenyl−NO_2 bonds to acquire significant double bond character. Note that generation of the methide species from chemisorbed NAB requires transfer of only 1 e^-, but that electron strongly affects the bond between the NAB and carbon. In the case of NAB chemisorbed to GC, this bond does not terminate with the methide, of course, but is coupled into the extended graphitic π system.

Inspection of Table 3 reinforces the conclusion that substantial structural rearrangement occurs upon NAB reduction, consistent with the major spectral changes. The decrease in the NO_2 and N═N intensities correlates with changes in the N−O, N═N, and C−NO_2 bond lengths. However, NAB anion is structurally similar to both NAB methide and phenyl-NAB anion in terms of bond lengths and local charge density. While it is clear that significant structural changes occur upon NAB reduction and upon transfer of an electron from GC to chemisorbed NAB, distinctions between a chemisorbed anion and the methide are not so clear. The calculated charge distributions, bond lengths, and vibrational frequencies for NAB^- are quite similar to those for NAB methide, with the exception of the charge on the 4′-carbon involved in bonding to the carbon surface. The delocalized structure shown in the lower right portion of Figure 11 incorporates the bonding changes upon reduction, with the methide and anion bonded to the graphitic π system corresponding to different resonance forms of the delocalized structure. A precedent for this structure is the product of the reaction of dinitrophenylhydrazine (DPNH) with carbonyl groups on GC surfaces. The spectroscopy of this adduct supports delocalized bonding with restricted rotation about the bond between the hydrazine nitrogen and the phenyl ring contained in the graphite plane.[22,53] A consequence of the structures of both the DNPH product and the reduced, chemisorbed NAB is a planar ring system, which is constrained to remain parallel to the graphitic planes in the glassy carbon.

The fact that the spectroscopic changes for GC−NAB occur over a wide range of potentials and the large width of the voltammetric peaks for chemisorbed NAB indicate that electron transfer occurs between the GC and NAB over an unusually broad potential range. Charge transfer does not appear to be governed by a Nernst relation, nor does it appear to be kinetically hindered. If electron transfer were slow, the cathodic and anodic peaks in the voltammogram would be separated in potential, more so at higher scan rate. Furthermore, the spectroelectrochemical experiments were very slow compared to the voltammograms, and should have permitted time for electron transfer to occur. Finally, the spectroscopic changes were largely reversible, as was the voltammetric cathodic and anodic charge, indicating equilibrium between the NAB monolayer and GC surface on the time scale of the experiments. These observations support the conclusion that electron transfer between NAB and GC is rapid on the time scale of spectrum acquisition and voltammetry, consistent with strong electronic

(51) Villegas, I.; Weaver, M. J. *J. Phys. Chem. B* **1997**, *101*, 5842.
(52) Doering, W. E.; Nie, S. *J. Phys. Chem. B* **2002**, *106*, 311.
(53) Fryling, M.; Zhao, J.; McCreery, R. L. *Anal. Chem.* **1995**, *67*, 967.

coupling across a conjugated phenyl−phenyl bond at the GC/NAB interface. In the limit of strong electronic coupling, the GC and chemisorbed NAB may be considered to be one electronic system, and the electric field from the applied potential causes partial redistribution of electrons within this system. As the GC potential becomes negative, electrons transfer to the NAB, but not as a discrete redox event such as would occur with a redox center in solution or bound with an insulating tether. For potentials negative of −800 mV, structural rearrangement occurs to form the quinoid structure, and "complete" transfer of 1 e^- occurs from GC to NAB. The covalent, conjugated bond between GC and NAB has the effect of softening the boundary between the graphitic conductor and chemisorbed NAB, thus making electron transfer a less discrete event. By analogy to the potential-dependent "chemical enhancement" of Raman scattering observed for adsorbates on metals, the spectroscopic changes observed for GC−NAB result from a redistribution of electrons in an electric field, which leads to structural rearrangement at sufficiently high fields. To reiterate, the NAB-modified GC surface behaves like one electronic system in the limit of strong electronic coupling, driven by the large electric field at the electrode/solution interface.

Acknowledgment. This work was supported by the Analytical and Surface Chemistry division of the National Science Foundation through Grant 9819978 and by the Air Force Office of Scientific Research through Grant F49620-96-1-04790.

JA020398U